ACS APPLIED NANO MATERIALS

Open Access

www.acsanm.org

Article

Electrical Characterization of Self-Assembled 1D Gold Nanoparticle Chains: Implications for Chemiresistor Sensors

Stefan M. Schupp, David J. Schupp, Holger Hilbert, Emil Schwarz, Rebecca Köser, Helmut Cölfen, and Lukas Schmidt-Mende*

Cite This: *ACS Appl. Nano Mater.* 2024, 7, 20775−20782

Read Online

ACCESS | Metrics & More | Article Recommendations | Supporting Information

ABSTRACT: The introduction of dipoles on gold nanoparticle surfaces provides the formation of chain-like nanoparticle assemblies in solution under ambient conditions. Here, we present studies on influencing and controlling the strength of the induced dipole by thiols. Aromatic thiols lead to enhanced surface dipoles, where electron-donating functions can further increase the interaction. Thereby, particle−particle distances and chemical environment at the particle interface were manipulated, which resulted in different tunneling resistances R_g in these 1D structures. Here, R_g seemed to be mostly dominated by the interparticle distance rather than the type of ligand. Temperature-dependent current−voltage measurements of thiol-bearing nanoparticle chains revealed two different transport mechanisms. For temperatures <170 K, a thermally activated electron tunneling takes place, which depends on the charging energy E_c. Whereas for higher temperatures, a transition to an electron hopping process occurs determined by the involved thiol and nanoparticle shape. For structures with strong interparticle electronic coupling, the conduction mechanism is almost temperature-independent, which makes them promising candidates for highly sensitive chemiresistor sensors.

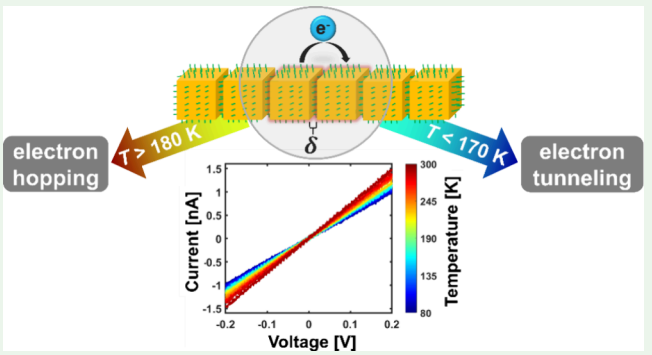

KEYWORDS: *anisotropic nanoparticles, gold, self-assembly, induced dipole, electrical conductivity, nanoprobing, Arrhenius*

INTRODUCTION

Self-assembly of inorganic nanoparticles is a promising approach for new and tailored nanomaterials. The bottom-up synthesis offers functional materials for different applications like electronic devices,[1] sensing,[2] catalysis,[3] or data storage.[4] There is a wide variety of available superstructures like strings,[5−7] helices,[8] sheets,[9] or vesicles.[10] Thereby, several researchers used a molecular polymerization model to predict and describe nanoparticle self-assemblies.[11,12] Speaking of gold nanoparticle assemblies, ligands with thiol functions are very prominent.[13,14] The well-known affinity of thiol groups to gold surfaces offers a perfect tool to control the nanoparticle interface. For oriented assembly of gold nanoparticles, a ligand-induced dipole mechanism was proposed.[15,16] The inhomogeneous distribution of ligands, adsorbates, or surfactants at the interface induces a dipole.[17] The formed dipoles will lead to a linear arrangement of the nanoparticles in order to minimize dipole−dipole repulsion. Here, the authors described the assembly globally as a first-order reaction. Surprisingly, the addition of surfactants to the destabilizing phase increases the speed of assembly drastically.[18] The dipole induction is favored by increased surfactant adsorption−desorption dynamics and leads to a step-growth mechanism of a second order. Goldmann et al. showed that plasmonic properties of gold nanoparticles can be influenced by thiol-containing aromatic ligands via an electron transfer at the hybrid interface.[19] The electron transfer is sensitive to the localized dipole moment of possible substituents in the aromatic system. Therefore, electron-withdrawing substituents such as halogens were found to decrease the Gibbs free energy of thiol adsorption.[20] Thereby, the dipole-driven assembly mechanism could be manipulated by using electron-withdrawing or -donating thiols, which may affect the dipole induction on the particle surfaces. To implement these 1D nanoparticle (NP) chains in future electronic devices, such as chemiresistor sensors,[21−24] it is necessary to understand their underlying conduction mechanism. Usually, extended 2D[25−28] or 3D[29−32] NP structures are electrically investigated. The used organic ligand drastically influences the electronic behavior due to different NP−NP distances, dielectric constants of the NP environment, and electronic coupling between the NPs.[29,30,33] However, there is

Received: June 28, 2024
Revised: August 8, 2024
Accepted: August 12, 2024
Published: August 19, 2024

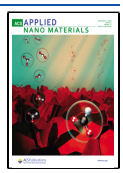

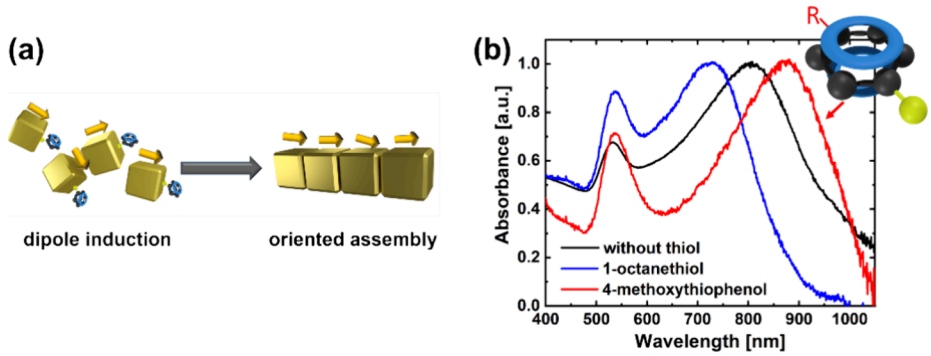

Figure 1. (a) Schematic illustration of a thiol-supported oriented assembly of gold nanocubes. By destabilizing the gold NPs, dipoles are induced at the surfaces. The thiols (here aromatic thiols) preferentially adsorb on {100} facets due to more frequent bridge sites and influence the surface dipoles at these facets. Thus, thiols can be used to manipulate the assembly process. (b) Comparison of UV−vis absorption spectra from cube chains assembled with different thiols (after 10 min of assembly). Aromatic thiols (red) result in a red-shifted LSPR band, and nonaromatic thiols (blue) lead to a blue-shifted LSPR band compared to gold NP chains assembled without additives (black). Insert upper right: illustration of a para-substituted aromatic thiol as 4-methoxythiophenol.

a lack of electronic studies of 1D NP structures, which are essential to reveal fundamental electron transport characteristics in these NP systems. In literature, only a few reports on conductivity measurements of these nanomaterials exist, which are usually performed on spherical NPs at room temperature.[34−36] Here, we present a study of anisotropic gold (Au) NPs surrounded by an organic ligand. The combination of a dipole-assisted self-assembly process in solution and the transfer on prefabricated nanoelectrodes enables the temperature-dependent electrical characterization of single 1D NP chains, which gives new insights into the electron transport of these assemblies.

RESULTS AND DISCUSSION

As previously reported, dipole induction at nanoparticle (NP) surfaces caused by an inhomogeneous distribution of surfactants (due to a solvent exchange from water to ethanol) leads to the formation of 1D NP structures within minutes.[18] Thereby, parameters such as size, shape, and temperature have great influence on the assembly. In the following, various thiols were investigated regarding their influence on the dipole-directed assembly of two different shaped gold NP types (cubes and truncated cuboctahedra (TOHs)) with a comparable diameter. Figure 1a illustrates the assembly process used to generate 1D nanoparticle structures in solution (oriented assembly) for gold nanocubes (NCs). The absorbance spectrum shown in Figure 1b demonstrates the strong influence of the different thiols. Due to the formation of chain-like nanoparticle structures, the transversal surface plasmon resonance (TSPR) band at around 530 nm resembles the width of the chains.[37] The red-shifted band in the spectra refers to the longitudinal surface plasmon resonance (LSPR) of the elongated structures and thereby correlates with the length of the NP chains. Here, the LSPR is also affected by the interparticle coupling, i.e., the NP−NP distance and ligand properties.[38] However, for the used NP size of ∼40 nm, it is assumed that these interparticle influences can be neglected. Consequently, the LSPR band shifts to bigger wavelengths for increasing chain lengths.[14,39] The wavelengths of the formed LSPR bands after 10 min of assembly are extracted from the respective UV−vis spectra (Figure S1) and are listed in Table 1. The findings indicate that nonaromatic thiols, like 1-octanethiol or 11-mercaptoundecanoic acid (MUA), which are commonly used for the assembly of gold nanoparticles,[14]

Table 1. Table of All Used Thiols for the Assembly of Gold Cubes Cube1 and the Maximum of the Respective LSPR Band after 10 min of Assembly[a]

used thiol	mesomeric/inductive effect of R[b]	wavelength of formed LSPR band
		805 nm[c]
1-octanethiol		727 nm
MUA		745 nm
4-chlorothiophenol	(+M)/−I	830 nm
4-nitrothiophenol	−M/−I	838 nm
4-methylthiophenol	+I	870 nm
4-methoxythiophenol	+M	885 nm
2-naphthalenethiol		889 nm

[a]The aromatic thiols lead to an increased redshift of the formed LSPR band, whereas nonaromatic thiols like 1-octanethiol and MUA result in a decreased redshift (compared to NC chains assembled without thiols). [b]Mesomeric or inductive effect refers to the functional group R in Figure 1b. [c]Reference: NC chains were assembled without thiols.

decrease the redshift of the LSPR band, whereas aromatic thiols (here 4-methoxythiophenol) significantly increase the redshift compared to the NC chains assembled without thiols. It should be noted that in contrast to the aromatic thiols and 1-octanethiol, MUA provides a nanoparticle cross-linking by hydrogen interactions.[14,40] Obviously, the electron density next to the thiol group has a great effect on the assembly process. Here, the positive inductive or mesomeric effects of the substitutes (4-methylthiophenol and 4-methoxythiophenol) result in the biggest redshifts of the LSPR band and thereby indicate the formation of longer NP chains. It should be noted that in the case of 4-chlorothiophenol, the +M effect is dominated by the negative inductive effect, which is typical for halogenated aromatic systems.[41]

However, the aromatic thiols cause significantly longer structures, which indicate the strong effect of the delocalized electrons next to the thiol function. Interestingly, the use of 2-naphthalenethiol also leads to a strongly increased redshift of the LSPR band. Again, the presence of delocalized electrons supports the assembly process, but in contrast to the other aromatic thiols, the polycyclic aromatic hydrocarbon provides an increased number of delocalized electrons. The chain formation supporting effect of the 2-naphthalenethiol is comparable to the 4-methoxythiophenol (+M effect) regarding

https://doi.org/10.1021/acsanm.4c03713
ACS Appl. Nano Mater. 2024, 7, 20775−20782

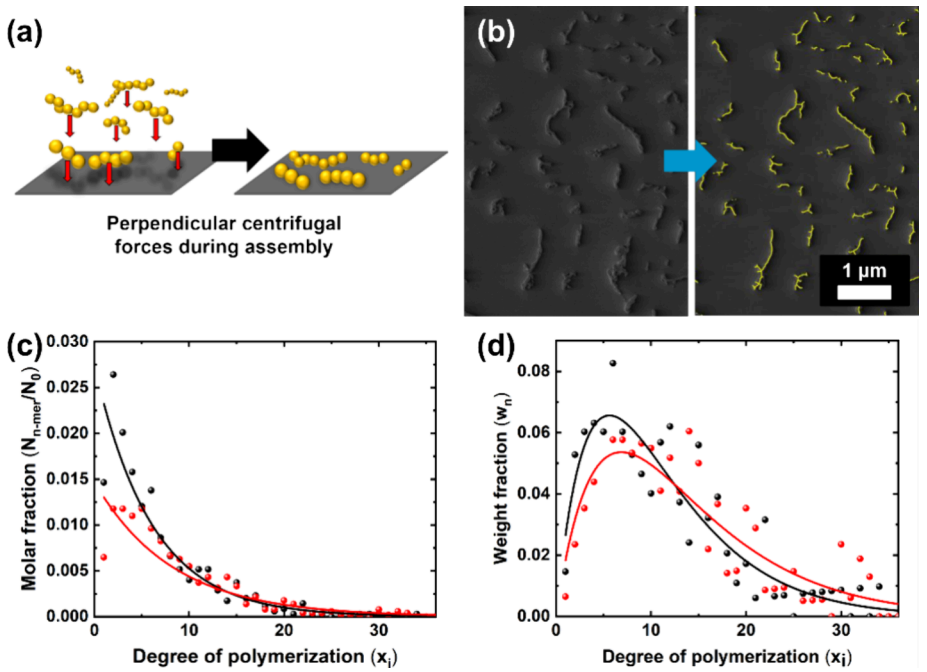

Figure 2. (a) Schematic principle of sample preparation. The formed NP chains are transferred to the substrate by centrifugal forces during the assembly process. (b) SEM image of assembled TOH chains (without aromatic thiol) on a silicon substrate overlaid with the corresponding image processing evaluation of the chains (yellow). (c) Molar and (d) weight fraction distributions for TOH chains assembled with aromatic thiols (4-methoxythiophenol; red curves) and without the addition of thiols (black curves) after 5 min. Here, the used models follow a Schulz−Flory distribution.

the redshift of the LSPR band. We conclude that the delocalized electrons in the aromatic system next to the gold surface-bound thiol function increase the induced surface dipole at the gold particles. In addition, electron-donating substituents result in stronger binding of the thiophenols to the gold surface. Thereby, enhancing the electron density in the aromatic system by electron-donating substituents is most effective to support the surface dipole-driven assembly. This agrees with findings of Emmons et al., who proposed that electron-withdrawing substituents, like halogens, decrease the binding of thiophenols to gold surfaces strongly.[20]

A comparison between assembled cubes and TOHs (Figure S2) indicates that they are strongly influenced by thiols. Nevertheless, the general effect of thiols on the TOH NP assembly is similar to the assembly of gold cubes. Nonaromatic thiols decrease the wavelength, whereas aromatic thiols increase the wavelength of the formed LSPR band of the TOH chains compared to the LSPR band of TOH chains assembled without aromatic thiols. Whereas NCs preferentially align via {100} facets, TOHs show alignment along the {100} and {111} facets. It was assumed that without thiols, the higher amount of possibilities for alignment in case of TOH particles (TOH particles have 14 possible contact faces, whereas NCs offer only 6) leads to the formation of longer chain-like structures,[18] which is resembled by a more red-shifted LSPR band ($LSPR_{TOH}$ band at around 850 nm (Figure S2a) versus $LSPR_{Cube}$ band at around 800 nm (Figure 1b)) and a higher LSPR/TSPR ratio for TOH chains (Figure S2b). However, when aromatic thiols are used within the assembly, the LSPR/TSPR ratio of the TOH chains is decreased significantly by 15.5%, whereas the LSPR/TSPR ratio of assembled NCs is only decreased by 3.5%. In addition, the use of 2-naphthalenethiol increases the LSPR redshift by 46 nm for TOHs and by 89 nm for NCs. Therewith, NCs and TOHs form longer structures accompanied by a decreased LSPR/TSPR ratio by the use of aromatic thiols, but the chain structure of the TOH assemblies is significantly more disturbed. In general, aromatic thiols preferentially adsorb to {100} facets due to the more frequently occurring bridge sites on these facets. Thereby, the adsorbed aromatic thiols prefer an upright orientation, which should be more favorable for the dipole induction.[42] Consequently, the presence of aromatic thiols during the assembly is more supportive for gold cubes and less supportive for TOHs by reducing the possible amount of assembly contributing faces.

To have a closer insight, complementary to the in situ investigation of the NP chains via UV−vis absorption spectroscopy, the formed TOH NP chains were investigated ex situ by electron microscope techniques. Therefore, growing nanoparticle chains were transferred after different assembly times onto silica substrates by the application of perpendicular centrifugal forces (Figure 2a). By doing so, the assembly is stopped immediately, and drying artifacts, such as agglomerates (Figure S4a), are reduced.[43] The recorded images of the chains were analyzed by a self-developed image processing algorithm.[43] Thereby, chain length distributions of the NP chains (Figure S4b) are available, which show chain lengths up to 1000 nm. Figure 2b displays a SEM image of the formed TOH chains (without aromatic thiol) after 5 min of reaction time and the corresponding image processing result. Here, the detected chains are colored yellow. Thus, the degree of polymerization distribution of the NP chains is determinable in molar (Figure 2c) and weight fraction (Figure 2d) in analogy to a classical polymerization (N_0 equals the amount of single gold particles, similar to a classical monomer, and $N_{n\text{-mer}}$ equals the number of chains with n particles). By presuming a Schulz−Flory distribution, typical polymerization parameters as the conversion can be calculated. Comparing the chain

https://doi.org/10.1021/acsanm.4c03713
ACS Appl. Nano Mater. 2024, 7, 20775−20782

length distribution of assembled TOHs after 5 min reaction time (Figure 2c,d), at which the assembly was performed in one case with thiols (4-methoxythiopenol) and without additional thiols in a second case, the assembly speed increasing influence of the aromatic thiol becomes visible. The conversion after 5 min is increased from 0.84 to 0.88 for 4-methoxythiophenols, and the maximum of the polymerization distribution (weight fraction) could be shifted toward higher values from 5.4 to 7.0. Even though the weight fraction weighted distribution exhibits a broader uncertainty and an inferior quality of the distribution fitting compared with the molar weighted distribution, the determined conversions are in good agreement. Thereby, the ex situ measurements confirm the in situ UV−vis data.

To investigate the electrical conductivity of the produced NP chains, tailored gold nanoelectrode structures were produced on silicon substrates with a thermal oxide layer. Subsequently, the NP chains were transferred to the substrate by centrifugal forces, which resulted in bridging of the nanosized electrodes. The electrodes consist of Cr/Au (3/50 nm) and have a spacing of 200−700 nm, matching the usual chain lengths as can be seen from the chain distribution in Figure S4b. A nanoprobing system transferred to a SEM chamber allows one to select the most linear Au NP structures and perform current−voltage (I−V) measurements (Figure S5). In this study, four different gold NP systems are investigated and compared, namely, TOHs with 2-naphthalenethiol (TOH_{NAP}), 4-methoxythiophenol (TOH_{MOP}) and without an additional aromatic thiol (TOH_{CPC}), and nanocubes (NCs) with 2-naphthalenthiol (NC_{NAP}). A test measurement of TOH_{NAP} chains showed that unwanted effects due to Joule heating, i.e., fusion or even destruction of the NP chains, can be avoided by keeping the voltage drop per NP below 20 mV (Figure S6). Under these conditions, all contacted NP assemblies show an ohmic and stable I−V behavior for the five applied measurement cycles with a vacuum resistance (R_{vac}) in the MΩ regime, as exemplarily shown for a TOH_{MOP} chain in Figure 3a,b. However, to account for branching effects and different chain lengths, the measured structures were approximated by a simplified equivalent circuit. Here, it is assumed that the measured resistance is dominated by the interparticle gap resistance R_g, while the resistance of Au NPs (<1 Ω per NP) can be neglected.[35] The contact resistance R_c is approached with half the gap resistance, i.e., $R_c = 1/2R_g$, assuming an organic single layer to be present between electrodes and contacted NPs.

This results in a total resistance of $R_{vac} \approx 11.1\ R_g$ (Figure 3c) for the displayed TOH_{MOP} chain. Therefore, the measured resistance of 269 ± 4 MΩ translates into a gap resistance of 24 MΩ. Typical I−V curves and respective equivalent circuits for the other NP systems are shown in Figures S7 and S8. This procedure was applied for five different chains of each NP system, which end up in the box plot, as shown in Figure 3d. The NPs with an aromatic thiol, namely, TOH_{NAP}, NC_{NAP}, and TOH_{MOP}, exhibit similar mean gap resistances of 31, 29, and 27 MΩ, respectively. Usually, the organic ligands surrounding the NPs act as a tunneling barrier for electron transport, which govern the current flow since $R_g \gg h/e^2 \approx 25.8$ kΩ.[26] Therefore, measured conductivities in such systems strongly depend on the length of ligands and the resulting interparticle distances.[22,26,30,44,45] In our study, TEM measurements (Figure S3) revealed an NP−NP distance of 1.4 ± 0.3 and 1.5 ± 0.3 nm for NPs covered with 2-naphthalenthiol and 4-methoxythiophenol, respectively, which is consistent with the similar gap resistances determined for TOH_{NAP}, NC_{NAP}, and TOH_{MOP}. These values are comparable to reported tunneling resistances for Au NPs separated by an organic thiol layer.[24,27,34,36,46] However, the mean gap resistance is drastically reduced for TOH_{CPC} with R_g = 365 kΩ. Here, the smaller interparticle distance of 0.8 ± 0.2 nm leads to almost 2 orders of magnitude higher conductivities compared to the previous NP systems. This change in resistance is in good agreement with previous considerations in the literature[24] and thus confirms well-separated NPs by an organic layer. Interestingly, the plasmonic properties of such NP chains seem to be strongly dependent on the ligand type, whereas their electrical resistance is mainly determined by the resulting interparticle distance.

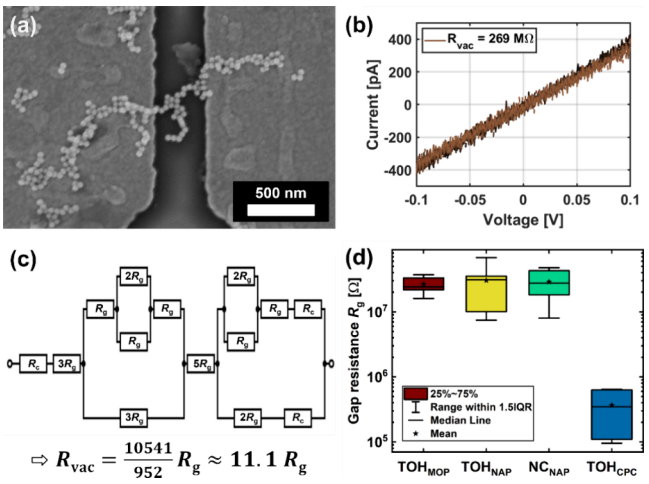

Figure 3. (a) SEM image of a TOH_{MOP} NP chain connected to prefabricated electrodes. (b) I−V measurements of the NP chain show an ohmic behavior for low voltages which results in the calculated resistance R_{vac}. (c) Schematic drawing of the simplified circuit for determining the gap resistance R_g. Here, contact resistance R_c is approximated with $1/2R_g$. (d) Box plot of the different NP types that displays a decrease of R_g for NP chains without an additional aromatic thiol.

All of these findings indicate an electron tunneling conduction mechanism occurring in these NP chains. Usually, a thermally activated hopping process wherein the thiolate layer acts as a tunneling barrier is assumed for such ordered systems.[28] Therefore, the inverse of measured resistance R follows[24,26,47,48]

$$\frac{1}{R} \propto e^{-2\delta\beta} e^{-E_a/k_B T} \tag{1}$$

where δ is the average interparticle distance, β is the electron tunneling coefficient, E_a is the activation energy for electron hopping between two neighboring NPs, k_B is the Boltzmann constant, and T is the applied temperature. For ordered structures, it can be assumed that a defined organic layer is present, i.e., thermal expansion is neglected, and δ and β are constants.[47] According to this, eq 1 can be simplified to

$$\frac{1}{R} = A e^{-E_a/k_B T} \tag{2}$$

with a temperature-independent prefactor A. The electrical resistance of single NP chains with aromatic thiols is measured for temperatures of 80−300 K to investigate the conduction mechanism in the different NP systems, namely, TOH_{NAP},

https://doi.org/10.1021/acsanm.4c03713
ACS Appl. Nano Mater. 2024, 7, 20775−20782

NC_{NAP}, and TOH_{MOP}. Several samples are measured per type to confirm the reproducibility of the transport characteristics. Typical Arrhenius plots are shown in Figure 4. Interestingly, all

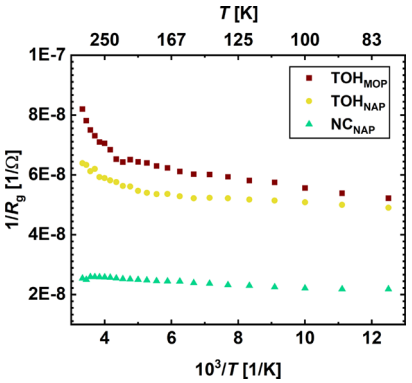

Figure 4. Arrhenius plots of investigated gold nanoparticle chains with an aromatic thiol at temperatures of 80−300 K.

samples showed an almost temperature-independent behavior for low temperatures, i.e., T < 170 K, with a similar linear slope. The activation energies in this low-temperature regime $E_{a,l}$ can be attributed to the charging energy E_c of the nanoparticles[26,28]

$$E_c = \frac{e^2}{2C_{tot}} \tag{3}$$

with the elementary charge e and total capacitance of the nanoparticle C_{tot}, which consists of the sum of self-capacitance and mutual capacitance.[30] For a linear NP chain with a nearest neighbor number of 2 and relative permittivity of ε_r = 4 (typical for aromatic compounds[46]), this ends up in a charging energy of ∼2.7 meV. Detailed calculations and discussions can be found in the Supporting Information (Supporting Information 2). This value is consistent with the activation energies obtained from the slope of the Arrhenius plot using eq 2 (Table 2). However, in our study, the associated Coulomb

Table 2. Extracted Activation Energies for the High-Temperature $E_{a,h}$ (>180 K) and Low-Temperature $E_{a,l}$ (<170 K) Regime for the Measured NP Chains in Figure 4

nanoparticle system	$E_{a,h}$ [meV]	$E_{a,l}$ [meV]
TOH_{MOP}	18	2.3
TOH_{NAP}	10	1.1
NC_{NAP}	2.6	2.2

blockade and the resulting asymmetric current−voltage behavior are not observable since the condition $E_c \gg k_BT$ (∼7 meV at 80 K) is not fulfilled.[26] Therefore, even for low temperatures, all measured samples showed an ohmic I−V behavior in the investigated voltage range. These findings imply a thermally activated tunneling mechanism in these NP systems for T < 170 K.[28]

More interestingly, the NP chains exhibit another activation energy for T > 180 K. In this temperature regime, ordered NP systems often show characteristics of an electron hopping mechanism.[26] It seems like the activation energy $E_{a,h}$ for this electron transport is decreased for 2-naphthalenethiol compared to that for 4-methoxythiophenol. A further decrease is observed if nanocubes are used instead of truncated cuboctahedra. In general, NCs mainly possess {100} facets, whereas the TOH particles have comparable surface amounts of {111} and {100} facets.[18] As previously discussed, Au{100} facets are more favorable for the adsorption of aromatic thiols. Therefore, the decrease in $E_{a,h}$ could imply an increased amount of adsorbed 2-naphthalenethiol for NC surfaces. Here, the preferred upright orientation and resulting $\pi-\pi$ stacking of the phenyl moieties lead to a strong interparticle electronic coupling.[21] Additionally, the NCs exhibit a larger interfacial area compared to TOHs, which should favor electron transfer and thus decrease energy barriers.[32] Consequently, these 1D structures exhibit almost no activation barrier throughout the entire temperature range, suggesting a tunneling-dominated conduction mechanism even at room temperature, which agrees with the literature.[21] A repeated temperature-dependent measurement of a NC_{NAP} chain confirmed that the observed transition of the conduction mechanism is an electronic characteristic of the NP system, which is independent of the applied temperature change, i.e., heating vs cooling (Figure S9). In the literature, a similar transition from a tunneling-dominated to hopping-dominated electron conduction mechanism for increasing temperatures was already observed by Stansfield and Thomas.[47] Here, the electronic properties of ordered Au nanocrystal films with a thickness of 100 nm consisting of ∼10 nm NPs surrounded by different thiophenol ligands are investigated. Their extracted activation energies for 4-methoxythiophenol are comparable to those presented here. This implies preservation of electronic properties from 3D to 1D structures for similar NP systems. In addition, such a transition in the conduction mechanism is reported for 2D monolayers of cobalt−platinum NPs with a diameter of 3.5 nm and oleylamine as ligand,[28] i.e., the observed transition in the conduction mechanism seems to be typical for ordered metal NP structures well-separated by an organic layer.

CONCLUSIONS

In summary, we have demonstrated a dipole-assisted self-assembly process that facilitates the formation of conductive chains composed of anisotropic gold nanoparticles. Specifically, aromatic thiols showed the formation of up to 1000 nm long chains due to the increased electron density at the surface of the NPs. The formed nanoparticle chains were electrically characterized by directly transferring them onto prefabricated electrodes. The systems investigated exhibit high resistance tunneling behavior, which is primarily dictated by the interparticle distance and independent of the aromatic thiol. However, temperature-dependent measurements revealed a shift from the thermally activated tunneling to hopping mechanism as the temperature increases from 80 to 300 K. Here, the observed activation energies for electron hopping are dependent on the shape of NPs and the ligands used. For NP assemblies with strong interparticle electronic coupling such as NC_{NAP} chains, this transition vanishes, and the conduction mechanism is dominated by tunneling throughout the entire temperature range. Thus, a chemiresistor sensor that is almost unaffected by the temperature can be achieved with these NP assemblies. Furthermore, the chain-like structure should result in outstanding sensitivities, which will be addressed in future work.

METHODS

Chemicals and Materials. Cetyltrimethylammonium bromide (CTAB) was purchased from Fisher Scientific, cetyltrimethylammo-

https://doi.org/10.1021/acsanm.4c03713
ACS Appl. Nano Mater. 2024, 7, 20775−20782

nium chloride 95% (CTAC) and 4-methoxythiophenol were purchased from abcr. Cetylpyridinium chloride (CPC), gold(III)-chloride trihydrate, 4-methylthiophenol, 4-nitrothiophenol, 11-mercaptodecanoic acid 95%, and 2-naphthalenethiol 99% were purchased from Sigma-Aldrich. Sodium borohydride and potassium bromide were purchased from Merck. Ethanol ≥99.8% p.a. and L-ascorbic acid p.a. were purchased from Carl Roth. 4-Chlorothiophenol >98% was bought from Fluka. Thiosalicylic acid 98% and 1-octanethiol 97% were purchased from ACROS.

Overview Particle Synthesis. The gold particles were synthesized by a three-step seed-mediated growth method (in analogy to the gold particle synthesis by Kirner et al.[49]), which was reported previously in detail.[18] In the first step, a seed solution was prepared by adding sodium borohydride to a cetyltrimethylammonium bromide (CTAB) solution and tetrachloroauric(III) acid. Afterwards, the seeds were added to a mixture of cetyltrimethylammonium chloride (CTAC) and tetrachloroauric(III) acid, resulting in small gold spheres. Finally, the gold spheres were injected into a growth solution consisting of cetylpyridinium chloride (CPC), tetrachloroauric(III) acid, ascorbic acid, and KBr.

Gold Seeds Synthesis. 0.6 mL of a chilled 0.01 M $NaBH_4$ (5−8 °C) was added to a vigorous stirred solution of 7.5 mL of 0.1 M CTAB and 0.25 mL of 0.01 M $HAuCl_4$ at 27 °C and aged for 1 h without stirring. The seeds were not purified and used immediately after synthesis.

Gold Spheres Synthesis. 39 g of 0.1 M CTAC and 1 mL of 0.01 M $HAuCl_4$ were tempered at 27 °C. Then, 15 mL of 0.01 M ascorbic acid (27 °C) and 200 μL of seeds were added to the stirred growth solution. The reaction mixture was allowed to stay overnight at 27 °C. Typically, 3 mL portions of spheres were centrifuged (9000 rpm/7690 rcf for 10 min); the slightly pink colored supernatant was removed, followed by the addition of 0.5 mL of a 0.1 M aqueous CPC solution. The resulting gold spheres (diameter: 19 nm) solution had a maximum absorbance of around 0.8 o.d. and were directly used for the synthesis of truncated cuboctahedra and cubes.

Gold Truncated Cuboctahedra Synthesis. Truncated cuboctahedra (TOHs) were synthesized by adding gold spheres solution to a growth solution consisting of 12.5 g of 0.1 M CPC, 1.25 mL of 0.1 M KBr, 0.25 mL of 0.01 M $HAuCl_4$, and 0.375 mL of 0.1 M ascorbic acid solution at 27 °C. It should be noted that the ascorbic acid was injected into the tempered growth solution 20 min before the gold spheres injection (100 μL of spheres solution). Then, the reaction mixture was allowed to stay for around 15 h at 27 °C. The resulting ∼38 nm-sized TOHs were centrifuged (9000 rpm/7690 rcf for 10 min; TOH1), the supernatant was removed, and the particle concentration was adjusted to 0.49 mg/mL by the addition of Milli-Q.

Gold Cubes Synthesis. The gold nanocubes (NCs) were synthesized at 27 °C by the addition of gold spheres to a growth solution. The growth solution consisted of 12.5 g of 0.1 M CPC, 0.25 mL of 0.1 M KBr, 0.25 mL of 0.01 M $HAuCl_4$ and 0.375 mL of 0.1 M ascorbic acid solution. The ascorbic acid was injected to the tempered growth solution 20 min before the gold spheres injection. Then, 300 μL of gold spheres were added to the growth solution which results in ∼40 nm-sized gold cubes (Cube1). The reaction was stopped after ∼15 h by centrifugation (9000 rpm/7690 rcf for 10 min) of the reaction mixture and removal of the supernatant. The NC concentration was adjusted to 0.49 mg/mL by the addition of Milli-Q.

NP Chain Synthesis. The particles were destabilized by solvent exchange. Therefore, the stabilized nanoparticles were injected into a CPC and respective thiol-containing ethanol solution. In a typical experiment, 62.5 μL of gold nanoparticles (0.49 mg/mL) were added to a mixture of 0.5 mL of CPC solution and 0.5 mL of 10 mM thiol solution (both solved in ethanol). The temperature was set to 22−23 °C.

Characterization Methods. To enable ex situ investigations of the NP chains by electron microscopy methods, scanning electron microscopy (SEM), and transmission electron microscopy (TEM), a silicon wafer (SEM) or carbon-supported copper grid (TEM) was placed in the reaction mixture. By applying perpendicular centrifugal forces (9000 rpm/7690 rcf for 2 min), the NP chains were transferred directly from the reaction mixture onto the respective substrate. The substrates were removed and washed with ethanol for a few seconds. By doing so, drying artifacts were reduced, and a representative snapshot of the assembly products could be achieved at different reaction times. TEM images were recorded with a Zeiss TEM Libra 120 operating at 120 kV, and SEM images were recorded with a Zeiss Gemini 500. UV−vis absorption measurements were executed with a Varian Cary 50 BIO UV−visible spectrophotometer. Dynamic light scattering (DLS) measurements were performed on a Malvern Zetasizer Nano ZSP.

Electrical Characterization. Silicon substrates with a 1 μm thick thermally grown silicon dioxide layer were cut into 13.8 × 13.8 mm^2 pieces and cleaned in deionized water, followed by acetone and isopropanol in an ultrasonic bath for 10 min each. Electron-beam and optical lithography processes were applied to generate Cr/Au (3 nm/50 nm) electrodes with a spacing of 200−700 nm and additional big gold contacts adapted to a measurement mask, respectively. The samples were placed in a vial with the respective nanoparticle−thiol mixture and centrifuged (2 min at 9000 rpm/7690 rcf). Hereby, formed NP chains were randomly deposited on the whole substrate. Afterward, the samples were transferred into a SEM chamber equipped with a nanoprobing system from Imina Technologies. Here, two individual miBot nanoprobers with tungsten tips (radius of 1 μm) were used to contact selected electrodes, which are bridged by a single linear NP chain. The tips were connected to a Keithley 2401, which can be controlled remotely by a MATLAB program to perform in situ current−voltage (I−V) measurements. The applied maximum voltage was chosen so that the voltage drop is less than 20 mV per NP to avoid any damage due to Joule heating effects. For each contact, five consecutive forward and backward I−V scans were performed to check for measurement stability. During electrical measurements, the electron beam was blocked to avoid influences of incident electrons. Temperature-dependent I−V measurements were performed in a cryostat in vacuum (pressure $<10^{-5}$ bar) cooled by liquid nitrogen (80−300 K). Previously, selected electrodes bridged by NP chains were contacted with the bigger electrodes by silver paste. To ensure equilibrium, the samples were kept at each temperature for 15 min before performing two forward and backward I−V sweeps with a Keithley 2401.

■ ASSOCIATED CONTENT

● Supporting Information

The Supporting Information is available free of charge at https://pubs.acs.org/doi/10.1021/acsanm.4c03713.

Additional UV−vis data of NP self-assembly with and without aromatic thiol; chain length distribution; TEM images of the different NP systems; sample layout for electrical characterization; I−V measurements of the other NP systems; used simplified equivalent circuits stability measurements; and detailed calculation and discussion of the charging energy (PDF)

■ AUTHOR INFORMATION

Corresponding Author

Lukas Schmidt-Mende − *Department of Physics, University of Konstanz, Konstanz 78457, Germany;* orcid.org/0000-0001-6867-443X; Email: lukas.schmidt-mende@uni-konstanz.de

Authors

Stefan M. Schupp − *Department of Physics, University of Konstanz, Konstanz 78457, Germany*

David J. Schupp − *Physical Chemistry, Department of Chemistry, University of Konstanz, Konstanz 78457, Germany*

https://doi.org/10.1021/acsanm.4c03713
ACS Appl. Nano Mater. 2024, 7, 20775−20782

Holger Hilbert − *Physical Chemistry, Department of Chemistry, University of Konstanz, Konstanz 78457, Germany;* orcid.org/0000-0003-3552-1036
Emil Schwarz − *Physical Chemistry, Department of Chemistry, University of Konstanz, Konstanz 78457, Germany*
Rebecca Köser − *Physical Chemistry, Department of Chemistry, University of Konstanz, Konstanz 78457, Germany*
Helmut Cölfen − *Physical Chemistry, Department of Chemistry, University of Konstanz, Konstanz 78457, Germany;* orcid.org/0000-0002-1148-0308

Complete contact information is available at: https://pubs.acs.org/10.1021/acsanm.4c03713

Author Contributions

S.M.S. and D.J.S. contributed equally to this paper. S.M.S. executed the whole electrical characterization including sample fabrication, electrical measurements, data analysis, and writing. D.J.S. carried out the NP synthesis, self-assembly, and characterization with assistance of E.S. and R.K. and conducted the analysis and writing of respective parts. H.H. programmed the used image processing algorithm. The manuscript was written through contributions of all authors. All authors have given approval to the final version of the manuscript.

Notes

The authors declare no competing financial interest.

■ ACKNOWLEDGMENTS

The authors thank the Deutsche Forschungsgemeinschaft (DFG) for financial support (project ID: 510996696). Furthermore, we acknowledge the Particle Analysis Center (PAC) and Nanolab at the University of Konstanz for providing various measurement equipment.

■ REFERENCES

(1) Nie, Z.; Petukhova, A.; Kumacheva, E. Properties and emerging applications of self-assembled structures made from inorganic nanoparticles. *Nature Nanotechnol.* **2010**, *5* (1), 15−25.
(2) Yan, Y.; Warren, S. C.; Fuller, P.; Grzybowski, B. A. Chemoelectronic circuits based on metal nanoparticles. *Nat. Nanotechnol.* **2016**, *11* (7), 603−608.
(3) Kang, Y.; Ye, X.; Chen, J.; Cai, Y.; Diaz, R. E.; Adzic, R. R.; Stach, E. A.; Murray, C. B. Design of Pt−Pd binary superlattices exploiting shape effects and synergistic effects for oxygen reduction reactions. *J. Am. Chem. Soc.* **2013**, *135* (1), 42−45.
(4) Klajn, R.; Wesson, P. J.; Bishop, K. J.; Grzybowski, B. A. Writing self-erasing images using metastable nanoparticle "inks. *Angew. Chem., Int. Ed.* **2009**, *48* (38), 7035−7039.
(5) Nie, Z.; Fava, D.; Kumacheva, E.; Zou, S.; Walker, G. C.; Rubinstein, M. Self-assembly of metal−polymer analogues of amphiphilic triblock copolymers. *Nature materials* **2007**, *6* (8), 609−614.
(6) Zhang, X.; Lv, L.; Wu, G.; Yang, D.; Dong, A. Cluster-mediated assembly enables step-growth copolymerization from binary nanoparticle mixtures with rationally designed architectures. *Chemical Science* **2018**, *9* (16), 3986−3991.
(7) Zhang, X.; Lv, L.; Ji, L.; Guo, G.; Liu, L.; Han, D.; Wang, B.; Tu, Y.; Hu, J.; Yang, D.; Dong, A. Self-assembly of one-dimensional nanocrystal superlattice chains mediated by molecular clusters. *J. Am. Chem. Soc.* **2016**, *138* (10), 3290−3293.
(8) Singh, G.; Chan, H.; Baskin, A.; Gelman, E.; Repnin, N.; Král, P.; Klajn, R. Self-assembly of magnetite nanocubes into helical superstructures. *Science* **2014**, *345* (6201), 1149−1153.
(9) Cheng, W.; Campolongo, M. J.; Cha, J. J.; Tan, S. J.; Umbach, C. C.; Muller, D. A.; Luo, D. Free-standing nanoparticle superlattice sheets controlled by DNA. *Nature materials* **2009**, *8* (6), 519−525.
(10) He, J.; Liu, Y.; Babu, T.; Wei, Z.; Nie, Z. Self-assembly of inorganic nanoparticle vesicles and tubules driven by tethered linear block copolymers. *J. Am. Chem. Soc.* **2012**, *134* (28), 11342−11345.
(11) Liu, K.; Nie, Z.; Zhao, N.; Li, W.; Rubinstein, M.; Kumacheva, E. Step-growth polymerization of inorganic nanoparticles. *science* **2010**, *329* (5988), 197−200.
(12) Ma, X.; Gu, M.; Zhang, L.; Lin, J.; Tian, X. Sequence-regulated supracolloidal copolymers via copolymerization-like coassembly of binary mixtures of patchy nanoparticles. *ACS Nano* **2019**, *13* (2), 1968−1976.
(13) Zhang, H.; Fung, K.-H.; Hartmann, J. r.; Chan, C. T.; Wang, D. Controlled chainlike agglomeration of charged gold nanoparticles via a deliberate interaction balance. *J. Phys. Chem. C* **2008**, *112* (43), 16830−16839.
(14) Thomas, K. G.; Barazzouk, S.; Ipe, B. I.; Joseph, S. S.; Kamat, P. V. Uniaxial plasmon coupling through longitudinal self-assembly of gold nanorods. *J. Phys. Chem. B* **2004**, *108* (35), 13066−13068.
(15) Liao, J.; Zhang, Y.; Yu, W.; Xu, L.; Ge, C.; Liu, J.; Gu, N. Linear aggregation of gold nanoparticles in ethanol. *Colloids Surf., A* **2003**, *223* (1−3), 177−183.
(16) Li, M.; Johnson, S.; Guo, H.; Dujardin, E.; Mann, S. A Generalized Mechanism for Ligand-Induced Dipolar Assembly of Plasmonic Gold Nanoparticle Chain Networks. *Adv. Funct. Mater.* **2011**, *21* (5), 851−859.
(17) Foerster, B.; Spata, V. A.; Carter, E. A.; Sönnichsen, C.; Link, S. Plasmon damping depends on the chemical nature of the nanoparticle interface. *Sci. Adv.* **2019**, *5* (3), No. eaav0704.
(18) Schupp, D. J.; Angst, J.; Schaefer, E. A.; Schupp, S. M.; Cölfen, H. Controlling Oriented Attachment of Gold Nanoparticles by Size and Shape. *J. Phys. Chem. C* **2021**, *125* (37), 20343−20350.
(19) Goldmann, C.; Lazzari, R.; Paquez, X.; Boissière, C.; Ribot, F.; Sanchez, C.; Chanéac, C.; Portehault, D. Charge transfer at hybrid interfaces: plasmonics of aromatic thiol-capped gold nanoparticles. *ACS Nano* **2015**, *9* (7), 7572−7582.
(20) Emmons, E. D.; Guicheteau, J. A.; Fountain, A. W.; Tripathi, A. Effect of substituents on surface equilibria of thiophenols and isoquinolines on gold substrates studied using surface-enhanced Raman spectroscopy. *Phys. Chem. Chem. Phys.* **2020**, *22* (28), 15953−15965.
(21) Segev-Bar, M.; Bachar, N.; Wolf, Y.; Ukrainsky, B.; Sarraf, L.; Haick, H. Multi-Parametric Sensing Platforms Based on Nanoparticles. *Adv. Mater. Technol.* **2017**, *2* (1), No. 1600206.
(22) Joseph, Y.; Besnard, I.; Rosenberger, M.; Guse, B.; Nothofer, H.-G.; Wessels, J. M.; Wild, U.; Knop-Gericke, A.; Su, D.; Schlögl, R.; Yasuda, A.; Vossmeyer, T. Self-assembled gold nanoparticle/alkanedithiol films: preparation, electron microscopy, XPS-analysis, charge transport, and vapor-sensing properties. *J. Phys. Chem. B* **2003**, *107* (30), 7406−7413.
(23) Cooper, J. S.; Raguse, B.; Chow, E.; Hubble, L.; Müller, K.-H.; Wieczorek, L. Gold nanoparticle chemiresistor sensor array that differentiates between hydrocarbon fuels dissolved in artificial seawater. *Analytical chemistry* **2010**, *82* (9), 3788−3795.
(24) Yang, C.-Y.; Li, C.-L.; Lu, C.-J. A vapor selectivity study of microsensor arrays employing various functionalized ligand protected gold nanoclusters. *Anal. Chim. Acta* **2006**, *565* (1), 17−26.
(25) Aleksandrovic, V.; Greshnykh, D.; Randjelovic, I.; Fromsdorf, A.; Kornowski, A.; Roth, S. V.; Klinke, C.; Weller, H. Preparation and electrical properties of Cobalt-Platinum nanoparticle monolayers deposited by the Langmuir-Blodgett technique. *ACS Nano* **2008**, *2* (6), 1123−1130.
(26) Greshnykh, D.; Fromsdorf, A.; Weller, H.; Klinke, C. On the electric conductivity of highly ordered monolayers of monodisperse metal nanoparticles. *Nano Lett.* **2009**, *9* (1), 473−478.
(27) Liao, J.; Bernard, L.; Langer, M.; Schönenberger, C.; Calame, M. Reversible Formation of Molecular Junctions in 2D Nanoparticle Arrays. *Adv. Mater.* **2006**, *18* (18), 2444−2447.

(28) Willing, S.; Lehmann, H.; Volkmann, M.; Klinke, C. Metal nanoparticle film−based room temperature Coulomb transistor. *Sci. Adv.* **2017**, *3* (7), No. e1603191.
(29) Schmid, G.; Simon, U. Gold nanoparticles: assembly and electrical properties in 1−3 dimensions. *Chem. Commun. (Camb)* **2005**, *6*, 697−710.
(30) Duan, C.; Wang, Y.; Sun, J.; Guan, C.; Grunder, S.; Mayor, M.; Peng, L.; Liao, J. Controllability of the Coulomb charging energy in close-packed nanoparticle arrays. *Nanoscale* **2013**, *5* (21), 10258−10266.
(31) Jenewein, C.; Schupp, S. M.; Ni, B.; Schmidt-Mende, L.; Cölfen, H. Tuning the Electronic Properties of Mesocrystals. *Small Sci.* **2022**, *2* (8), No. 2200014.
(32) Tsukiyama, K.; Takasaki, M.; Kitamura, N.; Idemoto, Y.; Oaki, Y.; Osada, M.; Imai, H. Enhanced oxide-ion conductivity of solid-state electrolyte mesocrystals. *Nanoscale* **2019**, *11* (10), 4523−4530.
(33) Kovalenko, M. V.; Scheele, M.; Talapin, D. V. Colloidal nanocrystals with molecular metal chalcogenide surface ligands. *Science* **2009**, *324* (5933), 1417−1420.
(34) Weiss, D. N.; Brokmann, X.; Calvet, L. E.; Kastner, M. A.; Bawendi, M. G. Multi-island single-electron devices from self-assembled colloidal nanocrystal chains. *Appl. Phys. Lett.* **2006**, *88* (14), 143507.
(35) Blech, K.; Noyong, M.; Juillerat, F.; Nakayama, T.; Hofmann, H.; Simon, U. In-situ electrical addressing of one-dimensional gold nanoparticle assemblies. *J. Nanosci Nanotechnol* **2008**, *8* (1), 461−465.
(36) Sato, T.; Ahmed, H.; Brown, D.; Johnson, B. F. G. Single electron transistor using a molecularly linked gold colloidal particle chain. *J. Appl. Phys.* **1997**, *82* (2), 696−701.
(37) Laza, S. C.; Sanson, N.; Sicard-Roselli, C.; Aghedu, A.; Palpant, B. Selective cold welding of colloidal gold nanorods. *Particle & Particle Systems Characterization* **2013**, *30* (7), 584−589.
(38) Willets, K. A.; Van Duyne, R. P. Localized surface plasmon resonance spectroscopy and sensing. *Annu. Rev. Phys. Chem.* **2007**, *58*, 267−297.
(39) Teulle, A.; Bosman, M.; Girard, C.; Gurunatha, K. L.; Li, M.; Mann, S.; Dujardin, E. Multimodal plasmonics in fused colloidal networks. *Nature materials* **2015**, *14* (1), 87−94.
(40) Ni, W.; Mosquera, R. A.; Pérez-Juste, J.; Liz-Marzán, L. M. Evidence for hydrogen-bonding-directed assembly of gold nanorods in aqueous solution. *J. Phys. Chem. Lett.* **2010**, *1* (8), 1181−1185.
(41) Reineke, W.; Knackmuss, H.-J. Chemical structure and biodegradability of halogenated aromatic compounds substituent effects on 1, 2-dioxygenation of benzoic acid. *Biochimica et Biophysica Acta (BBA)-General Subjects* **1978**, *542* (3), 412−423.
(42) Inagaki, M.; Motobayashi, K.; Ikeda, K. Electrochemical THz-SERS observation of thiol monolayers on Au (111) and (100) using nanoparticle-assisted gap-mode plasmon excitation. *J. Phys. Chem. Lett.* **2017**, *8* (17), 4236−4240.
(43) Schupp, D. J. Oriented Assembly and Attachment of Metal Nanoparticles. Ph.D. Thesis, University of Konstanz, 2021; pp 36−64. http://nbn-resolving.de/urn:nbn:de:bsz:352-2-ge1boky80yny4.
(44) Wessels, J. M.; Nothofer, H.-G.; Ford, W. E.; von Wrochem, F.; Scholz, F.; Vossmeyer, T.; Schroedter, A.; Weller, H.; Yasuda, A. Optical and electrical properties of three-dimensional interlinked gold nanoparticle assemblies. *J. Am. Chem. Soc.* **2004**, *126* (10), 3349−3356.
(45) Wang, G. R.; Wang, L.; Rendeng, Q.; Wang, J.; Luo, J.; Zhong, C.-J. Correlation between nanostructural parameters and conductivity properties for molecularly-mediated thin film assemblies of gold nanoparticles. *J. Mater. Chem.* **2007**, *17* (5), 457−462.
(46) Taniguchi, S.-i.; Minamoto, M.; Matsushita, M. M.; Sugawara, T.; Kawada, Y.; Bethell, D. Electron transport in networks of gold nanoparticles connected by oligothiophene molecular wires. *J. Mater. Chem.* **2006**, *16* (34), 3459−3465.
(47) Stansfield, G. L.; Thomas, P. J. Substituent effects on charge transport in films of Au nanocrystals. *J. Am. Chem. Soc.* **2012**, *134* (29), 11888−11891.
(48) Terrill, R. H.; Postlethwaite, T. A.; Chen, C.-h.; Poon, C.-D.; Terzis, A.; Chen, A.; Hutchison, J. E.; Clark, M. R.; Wignall, G. Monolayers in three dimensions: NMR, SAXS, thermal, and electron hopping studies of alkanethiol stabilized gold clusters. *J. Am. Chem. Soc.* **1995**, *117* (50), 12537−12548.
(49) Kirner, F.; Potapov, P.; Schultz, J.; Geppert, J.; Müller, M.; González-Rubio, G.; Sturm, S.; Lubk, A.; Sturm, E. Additive-controlled synthesis of monodisperse single crystalline gold nanoparticles: interplay of shape and surface plasmon resonance. *Journal of Materials Chemistry C* **2020**, *8* (31), 10844−10851.

https://doi.org/10.1021/acsanm.4c03713
ACS Appl. Nano Mater. 2024, 7, 20775−20782